

Suzaku OBSERVATION OF THE GIANT RADIO GALAXY 3C 326

NAOKI ISOBE ¹, MAKOTO S. TASHIRO ², POSHAK GANDHI ³, ASAMI HAYATO ³, HIROSHI NAGAI ⁴, KAZUHIRO HADA ⁵, HIROMI SETA ², KEIKO MATSUTA ⁶

ABSTRACT

A *Suzaku* observation of a giant radio galaxy, 3C 326, which has a physical size of about 2 Mpc, was conducted on 2008 January 19 – 21. In addition to several X-ray sources, diffuse emission was significantly detected associated with its west lobe, but the east lobe was contaminated by an unidentified X-ray source WARP J1552.4+2007. After careful evaluation of the X-ray and Non X-ray background, the 0.4 – 7 keV X-ray spectrum of the west lobe is described by a power-law model modified with the Galactic absorption. The photon index and 1 keV flux density was derived as $\Gamma = 1.82_{-0.24}^{+0.26} \pm 0.04$ and $S_X = 19.4_{-3.2}^{+3.3} \pm 3.0$ nJy, respectively, where the first and second errors represent the statistical and systematic ones. The diffuse X-rays were attributed to be inverse Compton radiation by the synchrotron radio electrons scattering off the cosmic microwave background photons. This radio galaxy is the largest among those with lobes detected through inverse Compton X-ray emission. A comparison of the radio to X-ray fluxes yields the energy densities of electron and magnetic field as $u_e = (2.3 \pm 0.3 \pm 0.3) \times 10^{-13}$ ergs cm⁻³ and $u_m = (1.2_{-0.1}^{+0.2} \pm 0.2) \times 10^{-14}$ ergs cm⁻³, respectively. The galaxy is suggested to host a low luminosity nucleus with an absorption-corrected 2 – 10 keV luminosity of $< 2 \times 10^{42}$ ergs s⁻¹, together with a relatively weak radio core. The energetics in the west lobe of 3C 326 were compared with those of moderate radio galaxies with a size of ~ 100 kpc. The west lobe of 3C 326 is confirmed to agree with the correlations for the moderate radio galaxies, $u_e \propto D^{-2.2 \pm 0.4}$ and $u_m \propto D^{-2.4 \pm 0.4}$, where D is their total physical size. This implies that the lobes of 3C 326 are still being energized by the jet, despite the current weakness of the nuclear activity.

Subject headings: radiation mechanisms: non-thermal — magnetic fields — X-rays: galaxies — radio continuum: galaxies — galaxies: individual (3C 326)

1. INTRODUCTION

Lobes of many kinds of radio sources, including radio galaxies, are the energy storehouse on a large scale in the universe, of non-thermal electrons and magnetic fields, both of which are conveyed from their active nuclei by the jets. In the course of the progress of the jets, the lobes expand with an estimated expansion velocity of about $0.01c - 0.1c$, where c is the speed of light, from a size of sub-kpc (e.g., Nagai et al. 2006) to ~ 100 kpc (e.g., Alexander & Leahy 1987) on a time scale of about 1 – 10 Myr. Therefore, investigation of the energetics in lobes, with respect to their size and/or age is thought to provide an important clue to probe into the history of the jet activity in the past.

X-ray observations of inverse Compton (IC) emission from non-thermal electrons in lobes, in which the cosmic microwave background (CMB) radiation plays role of a dominant seed photon source, are one of the ideal tools to examine the lobe energetics, because a comparison between the synchrotron radio and IC X-ray fluxes makes it

possible to evaluate precisely the energy densities of electrons and magnetic fields, u_e and u_m respectively (Harris & Grindlay 1979). Motivated by the pioneering discoveries of lobe IC X-rays with *ROSAT* and *ASCA* from Fornax A (Feigelson et al. 1995; Kaneda et al. 1995; Tashiro et al. 2001) and Centaurus B (Tashiro et al. 1998), several subsequent studies with *Chandra* (e.g., Isobe et al. 2002; Croston et al. 2005; Kataoka & Stawarz 2005) and *XMM-Newton* (e.g., Isobe et al. 2005, 2006; Migliori et al. 2007) proved the usefulness of this technique. Moreover, such research has revealed an electron dominance of $u_e/u_m = 1 - 10$ typically in lobes of moderate radio galaxies (e.g., Isobe et al. 2002; Croston et al. 2005).

The current IC results were limited to those from lobes of radio galaxies with a total size in a relatively narrow range of 50 – 500 kpc. In order to investigate the progress of lobe energetics, we urgently need to extend the size range of our sample. However, considering the angular resolution of the operating X-ray observatories (e.g., $\sim 0.5''$ for *Chandra* which corresponds to ~ 1 kpc at a redshift of $z \sim 0.1$), it is thought to be not easy to observe smaller ones. Therefore, we focused on radio galaxies, already evolved to more than 1 Mpc. These are called *giant radio galaxies* (e.g., Klein et al. 1994). Recently, Konar et al. (e.g., 2009) reported the *XMM-Newton* result on the giant radio galaxy 3C 457, of which the lobes exhibit a magnetic field by a factor of ~ 2 weaker than that under the minimum energy assumption.

For such X-ray sources extended on a large angular scale (e.g., $> 10'$ corresponding to ~ 1 Mpc at $z \sim 0.1$), *Suzaku* (Mitsuda et al. 2007) has a great advantage over the other X-ray observatories, thanks to its low and sta-

¹ Department of Astronomy, Kyoto University, Kitashirakawa-Oiwake-cho, Sakyo-ku, Kyoto 606-8502, Japan

Electronic address: n-isobe@kusaastro.kyoto-u.ac.jp

² Department of Physics, Saitama University, 255 Shimo-Ookubo, Sakura-ku, Saitama, 338-8570, Japan.

³ Cosmic Radiation Laboratory, the Institute of Physical and Chemical Research, 2-1 Hirosawa, Wako, Saitama, 351-0198, Japan

⁴ National Astronomical Observatory of Japan, 2-21-1 Osawa, Mitaka, Tokyo 181-8588, Japan

⁵ The Graduate University for Advanced Studies (SOKENDAI), 2-21-1 Osawa, Mitaka, Tokyo 181-8588, Japan

⁶ The Graduate University for Advanced Studies (SOKENDAI), 3-1-1 Yoshinodai, Sagamihara, Kanagawa, 229-8510, Japan

ble background (Tawa et al. 2008; Fukazawa et al. 2009) and its large effective area up to more than 10 keV. Actually, Tashiro et al. (2009) have confirmed IC X-ray emission from the west lobe of Fornax A, in a wider energy range up to ~ 20 keV, with a higher accuracy.

Located at the redshift of $z = 0.0895$ (Spinrad et al. 1985), 3C 326 is a giant radio galaxy with an elliptical host (Tremblay et al. 2007). It is classified as a narrow line radio galaxy (NLRG). Its radio images (e.g., Mack et al. 1997, 1998) revealed a lobe-dominant Fanaroff-Riley (FR) II morphology (Fanaroff & Riley 1974). The radio structure of 3C 326 has a total angular size of $20'.1$, corresponding to 1.99 Mpc at the source rest frame, which makes the object one of the largest radio sources in the universe. The object has a relatively high radio intensity of 7.4 ± 0.1 Jy at 609 MHz (Mack et al. 1997), which ensures a high IC X-ray flux, in combination with its large physical size. These encouraged us to select this radio galaxy as a target for a *Suzaku* observation.

We adopted the cosmological constants of $H_0 = 71$ km s^{-1} Mpc $^{-1}$, $\Omega_m = 0.27$, and $\Omega_\lambda = 0.73$. In this cosmology, 1 arcmin corresponds to 99.0 kpc, at the redshift of 3C 326.

2. OBSERVATION AND DATA REDUCTION

The *Suzaku* observation of the giant radio galaxy 3C 326 was performed on 2008 January 19 – 21. The X-ray Imaging spectrometer (XIS; Koyama et al. 2007) and the Hard X-ray Detector (HXD; Takahashi et al. 2007; Kokubun et al. 2007) onboard *Suzaku* were operated in the normal clocking mode without any window option, and in the normal mode, respectively. The optical host galaxy of 3C 326 was placed at the XIS nominal position for the X-ray telescope (XRT; Serlemitsos et al. 2007), so that almost all the radio structure ($20'.1$) was within the XIS field of view (a $17'.8 \times 17'.8$ square).

We reduced and analysed the data with the standard software package, HEASOFT 6.5.1. All the data were reprocessed, referring to the CALDB as of 2008 July 9. In the following, we concentrate on the XIS data, since hard X-ray signals from the target were not detected significantly with the HXD. The following criteria were adopted for the data screening; the spacecraft is outside the south Atlantic anomaly (SAA), the time after an exit from the SAA is larger than 436 s, the geometric cut-off rigidity is higher than 6 GV, the source elevation above the rim of bright and night Earth is higher than 20° and 5° , re-

spectively, and the XIS data are free from telemetry saturation. These procedures yielded about 50 ks of good exposure. In the scientific analysis below, we utilize only those events with a grade of 0, 2, 3, 4, or 6.

3. RESULTS

3.1. X-ray image

Figure 1 shows the 0.5 – 5 keV *Suzaku* XIS image of the 3C 326 field, on which a 1.4 GHz radio contour image (Leahy et al. unpublished) is overlaid. At the position of the host galaxy, (R.A., Dec) = ($15^h52^m09^s.19$, $+20^\circ05'23''.2$) in the J2000.0 coordinate (the star in Figure 1), we detected no bright X-ray source, while we found only a faint X-ray emission around it.

The XIS field of view (FoV) is rather crowded with several contaminating X-ray sources. The brightest point-like source detected at a J2000.0 coordinate of (R.A., Dec) = ($15^h52^m29^s.02$, $+20^\circ07'16''.2$) corresponds to a ROSAT source WARP J1552.4+2007 (Perlman et al. 2002). No definite counterpart for the object has been reported at any other wavelength. We noticed another bright point-like source, a quasar [HB89] 1543+203 with a redshift of $z = 0.25$ (Wegner & Swanson 1990), at (R.A., Dec) = ($15^h52^m01^s.61$, $+20^d13'57''.5$). There is a cluster of galaxies, WARP J1552.2+2013 (Perlman et al. 2002) with a redshift of $z = 0.136$ (Vikhlinin et al. 1998), on the north of 3C 326, where a diffuse X-ray structure is clearly detected.

In addition to these bright X-ray sources, a diffuse faint X-ray emission was detected from the west lobe of 3C 326. The spatial extent of the diffuse X-ray emission appears to be similar to that of the radio structure of the west lobe. On the contrary, severe contamination from WARP J1552.4+2007 prevented us to investigate X-ray emission from the east lobe.

3.2. X-ray spectrum of the source free region

Because the X-ray emission from the west lobe has a fairly low surface brightness, it is of crucial importance to evaluate precisely both X-ray and Non X-ray backgrounds (XRB and NXB, respectively). It is reported that the HEADAS tool `xisnxbgen` reproduces the NXB spectrum with a systematic uncertainty of better than $\sim 3\%$ in the 1 – 7 keV range, for a 50 ks exposure (Tawa et al. 2008).

It is widely known that the XRB spectrum in the 0.2 – 10 keV range is decomposed into a hard power-law (PL) component with a photon index of $\Gamma = 1.41$ and a two-temperature soft thermal plasma one (Kushino et al. 2002; Lumb et al. 2002). The hard PL component is thought to be dominated by unresolved faint sources, such as distant active galactic nuclei, and exhibits a small fluctuation in its flux ($\lesssim 7\%$; Kushino et al. 2002). On the other hand, the soft thermal component, which shows a significant field-to-field intensity variation, is thought to be associated with our Galaxy.

The XRB spectrum in this field was extracted from the source free region within the FoV (the square denoted as **SF** in Figure 1), without the known X-ray source regions (dashed circles). Figure 2 displays the XIS spectrum of the XRB, after the NXB, estimated by `xisnxbgen`, was subtracted. Because the SF region is irradiated with a radioactive calibration source (^{55}Fe) for the XIS FIs

TABLE 1

BEST-FIT SPECTRAL PARAMETERS OF THE SOURCE FREE REGION.

Parameter	Value
N_{H} (10^{20} cm $^{-2}$)	3.84 ^a
Γ	1.41 ^b
f_{hard} (ergs cm $^{-2}$ s $^{-1}$ sr $^{-1}$) ^c	$(6.0 \pm 0.5) \times 10^{-8}$
kT_1 (keV)	$0.33^{+0.21}_{-0.07}$
kT_2 (keV)	$0.11^{+0.04}_{-0.02}$
f_{soft} (ergs cm $^{-2}$ s $^{-1}$ sr $^{-1}$) ^d	$(2.5 \pm 0.2) \times 10^{-8}$
$\chi^2/\text{d.o.f}$	60.6/54

^aFixed at the Galactic value.

^bTaken from Kushino et al. (2002).

^cThe observed 2 – 10 surface brightness of the PL component

^dThe observed 0.5 – 2 keV surface brightness of the sum of the 2 MEKAL components

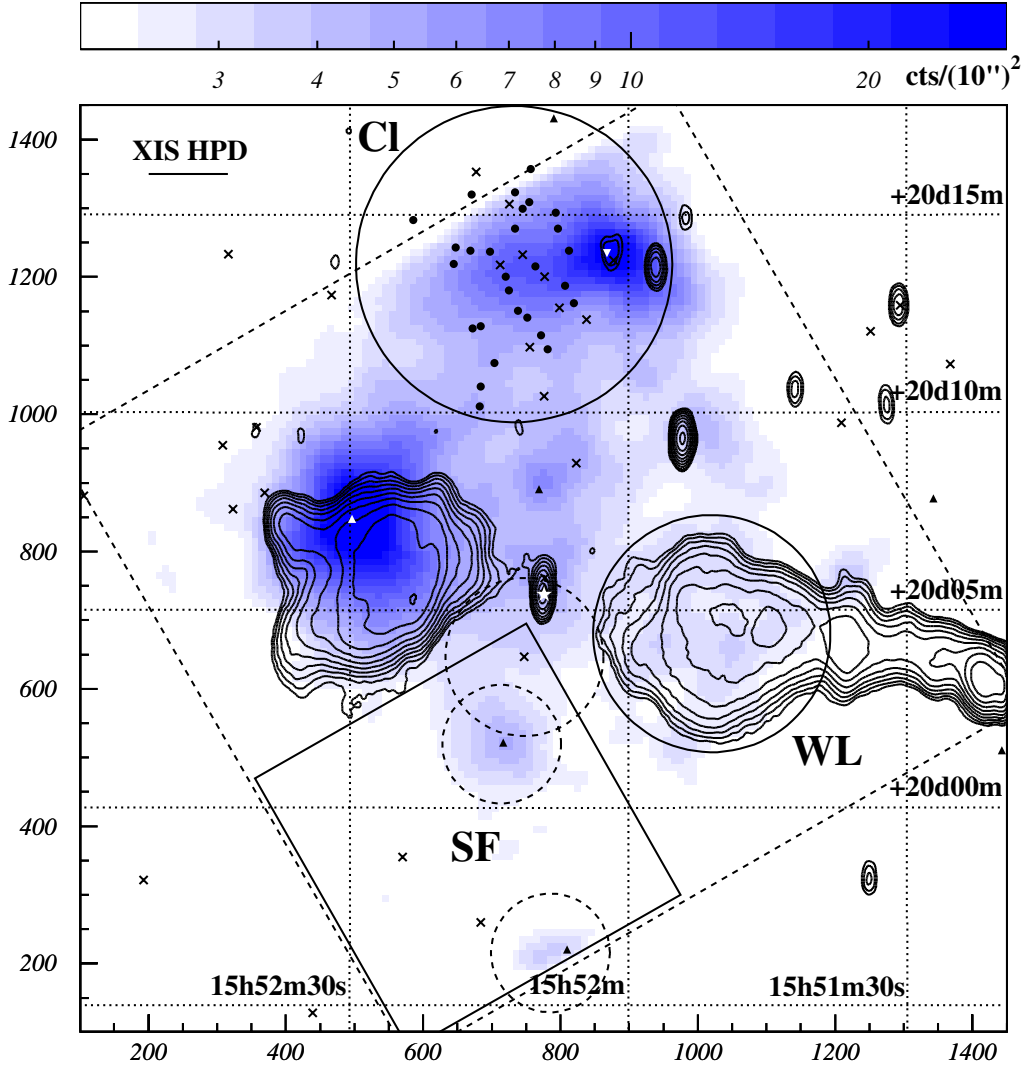


FIG. 1.— A blue-scale *Suzaku* XIS image of 3C 326 in 0.5 – 5 keV, smoothed with a two-dimensional Gaussian function of a 20'' radius. Contours are overlaid from a 1.4 GHz radio image (Leahy et al. unpublished). The scale bar on the top indicates the integrated X-ray counts within a 10'' \times 10'' bin. The XIS FoV is shown with the dashed square. The solid line at the top-left corner shows the point spread function of the XIS, with a typical half power diameter (HPD) of ~ 2 arcmin (Serlemitsos et al. 2007). The white filled star denotes the position of the optical host galaxy of 3C 326. Member galaxies of the cluster WARP J1552.2+2013 are referred by filled circles, and other galaxies by crosses. Black triangles corresponds to X-ray sources, taken from NED. The white normal and inverted triangles indicate the positions of WARP J1552.4+2007 and [HB89] 1543+203, respectively. X-ray signals of the west lobe, source free region and the cluster WARP J1552.2+2013 were accumulated from the regions denoted as **WL**, **SF** and **CI**, respectively. From the SF region, the dotted circles, corresponding to known X-ray sources, were removed.

(Koyama et al. 2007), we restricted the FI data below 5.5 keV. Consequently, the XRB signals were significantly detected in the 0.4 – 5 keV range.

Referring to the method in Kushino et al. (2002), we approximated the shape of the observed XRB spectrum. A composite model was adopted, consisting of a hard PL component and two soft MEKAL (e.g.; Mewe et al. 1985) ones, all of which were subjected to a photoelectric absorption with the Galactic hydrogen column density ($N_{\text{H}} = 3.84 \times 10^{20} \text{ cm}^{-2}$; Dickey & Lockman 1990). The photon index of the PL component was fixed at $\Gamma = 1.41$, while the MEKAL temperatures were both left free. Because the result was found to be insensitive to the met-

ality of the MEKAL components, we adopted the solar abundance ratio. We calculated response matrix functions (rmf) using `xisrmfgen`. Auxiliary response files (arf) were generated by `xissimarfgen` (Ishisaki et al. 2007), assuming a diffuse source with a 20' radius and a flat surface brightness distribution.

The model became acceptable ($\chi^2/\text{d.o.f} = 60.6/54$), with the parameters summarised in Table 1. The temperatures of the hot and cool MEKAL components are both reasonable (Lumb et al. 2002), at $kT_1 = 0.33^{+0.21}_{-0.07}$ keV and $kT_2 = 0.11^{+0.04}_{-0.02}$ keV, respectively. The observed 0.5 – 2 keV surface brightness of the sum of the thermal components was measured to be $f_{\text{soft}} = (2.5 \pm 0.2) \times 10^{-9}$ ergs

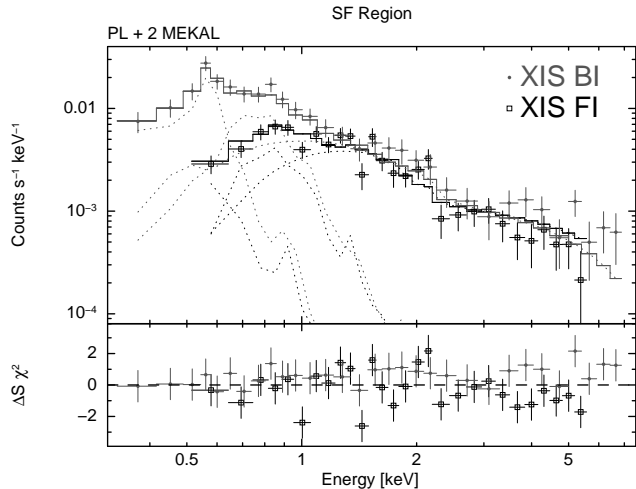


FIG. 2.— *Suzaku* XIS spectrum of the SF region without removing instrumental response, shown after the NXB events were subtracted. The best-fit model, consisting of a hard PL component and two soft MEKAL ones (dotted lines), is indicated by histograms in the top panel, while the residuals to the model are displayed in the bottom panel.

$\text{cm}^{-2} \text{s}^{-1} \text{sr}^{-1}$. We confirmed that the surface brightness of the hard PL component, which was determined as $f_{\text{hard}} = (6.0 \pm 0.5) \times 10^{-8} \text{ ergs cm}^{-2} \text{s}^{-1} \text{sr}^{-1}$ in the 2 – 10 keV range, was consistent with the result of Kushino et al. (2002), $f_{\text{hard}} = (6.4 \pm 0.6) \times 10^{-8} \text{ ergs cm}^{-2} \text{s}^{-1} \text{sr}^{-1}$, within the systematic field-to-field uncertainties ($\lesssim 7\%$; Kushino et al. 2002).

3.3. X-ray spectrum of the west lobe

The X-ray spectrum of the west lobe was integrated within the circle **WL** in Figure 1, with a radius of 3' (297 kpc in physical size). In Figure 3 (a), we show it in the 0.4 – 7 keV range, after subtracting only the NXB events in the manner similar to the X-ray spectrum of the SF region. The signal count rate over the NXB in the 0.4 – 7 keV was measured as $(1.22 \pm 0.04) \times 10^{-2} \text{ cts s}^{-1}$ and $(1.88 \pm 0.07) \times 10^{-2} \text{ cts s}^{-1}$ per CCD chip with the XIS FI and BI, respectively.

Adopting the best-fit XRB model spectrum determined from the SF region, we estimated the XRB count rate to be $0.75 \times 10^{-2} \text{ cts s}^{-1}$ and $1.22 \times 10^{-2} \text{ cts s}^{-1}$, within the WL region. Here, we precisely took into account the effect that the effective area to the XRB of the WL region is 0.5 – 0.9 times that of the SF region in the 0.5 – 7 keV. Thus, excess signals were significantly detected from the west lobe above the XRB spectrum, with a FI and BI count rate of $(0.47 \pm 0.04) \times 10^{-2} \text{ cts s}^{-1}$ and $(0.66 \pm 0.07) \times 10^{-2} \text{ cts s}^{-1}$, respectively. The excess is clearly visualised in Figure 3 (b), which show the residual spectrum ($\chi^2/\text{d.o.f} = 263.6/57$) of the west lobe over the XRB model. The excess count rate is higher than the uncertainty of the XRB model ($\sim 8\%$), derived in this observation.

In order to evaluate the excess spectrum from the west lobe, another PL component was introduced over the XRB model (XRB+PL). We generated the arf to the new PL component, assuming the west lobe to be a spatially uniform X-ray source with a 3' radius. Because the absorption column density to this component was uncon-

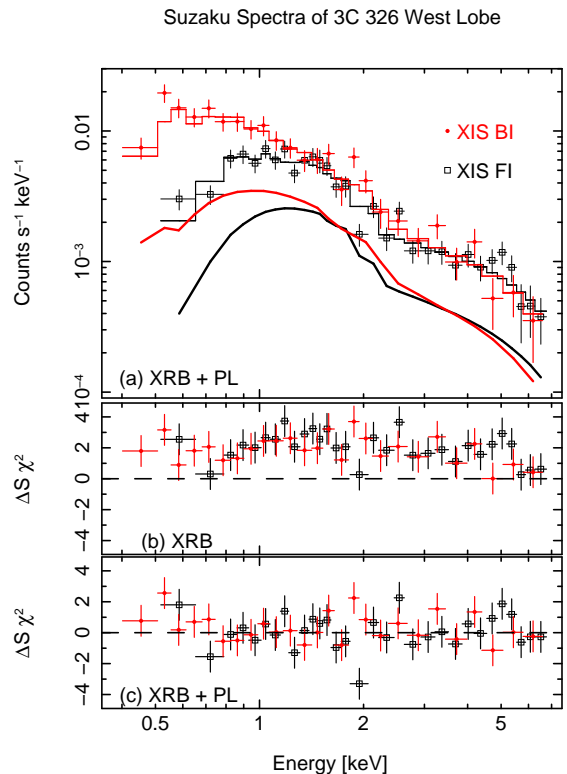


FIG. 3.— *Suzaku* XIS spectrum of the west lobe of 3C 326, shown after only the NXB were subtracted. The histograms in Panel (a) show the best-fit XRB+PL model, with the PL component indicated by the thick lines. Panels (b) and (c) show the residuals to the XRB model, and those to the best-fit XRB+PL model, respectively.

strained, we fixed it at the Galactic value. The additional PL component successfully reproduced the excess spectrum ($\chi^2/\text{d.o.f} = 61.9/55$), as shown in Figure 3 (c). We show the best-fit PL component with thick lines in Figure 3 (a), and its spectral parameters in Table 2 (Case 1). The photon index and flux density at 1 keV were determined to be $\Gamma = 1.82^{+0.26}_{-0.24}$ and $S_X = 19.4^{+3.3}_{-3.2} \text{ nJy}$. These correspond to a 0.5 – 10 keV absorption-corrected X-ray flux of $F_X = 1.7^{+0.1}_{-0.2} \times 10^{-13} \text{ ergs cm}^{-2} \text{s}^{-1}$.

The uncertainty of the XRB model, obtained from the SF region, can affect the spectral parameters of the excess signals from the west lobe. Therefore, we re-analysed the X-ray spectrum of the WL region, by changing the flux of the XRB model by $\pm 8\%$, which corresponds to the uncertainty in our analysis (see Table 1). As a result, we evaluated the uncertainty in the 1 keV flux density of the PL component as $\Delta S_X = 3.0 \text{ nJy}$, while we found that its photon index stayed relatively unchanged with an error of $\Delta\Gamma = 0.04$.

The west lobe could be contaminated by an extended X-ray emission from the cluster WARP J1552.2+2013 on the north of 3C 326 and/or other X-ray sources. However, as shown in Figure 1, there are no member galaxies of WARP J1552.2+2013 nor known X-ray sources within the west lobe. In order to investigate the possibility of the contamination from the cluster quantitatively, we re-analysed the X-ray spectrum of the west lobe, by replacing the PL model with a MEKAL one, of which temperature and metal abundance were both fixed at the best-fit

TABLE 2
SPECTRAL PARAMETERS OF THE WEST LOBE OF 3C 326

	Case 1	Case 2
N_{H} (10^{20} cm $^{-2}$)		3.84 ^a
Γ ^c	$1.82^{+0.26}_{-0.24} \pm 0.04$	1.8 ^b
S_{X} (nJy) ^c	$19.4^{+3.3}_{-3.2} \pm 3.0$	$19.3 \pm 2.2 \pm 2.6$
$\chi^2/\text{d.o.f}$	61.9/55	61.9/56

^aFixed at the Galactic value.

^bFixed at the synchrotron radio index.

^cThe first and second errors represent the statistical and systematic ones.

value for the cluster emission ($kT = 4.1$ keV and $A = 0.58$, respectively; see §3.5.3 for the details). However the fit became significantly worse ($\chi^2/\text{d.o.f.} = 69.5/56$) in comparison with the PL model. For the lobe spectrum, the PL model is supported rather than the cluster thermal emission, at an F-test confidence level of $\sim 99\%$. Therefore, we safely ascribed the diffuse X-ray emission to that from the west lobe itself.

3.4. X-ray spectrum of the host galaxy of 3C 326

We derived X-ray signals associated with the host galaxy of 3C 326, including its nucleus, from a circle centered on it (the filled star in Figure 1). In order to avoid the contamination from the lobes and a bright unidentified X-ray source WARP J1552.4+2007, a relatively small radius of $1.5'$ (149 kpc at the source rest frame) was adopted. As a sum of the NXB and XRB, we simply subtracted the X-ray spectrum of the SF region,

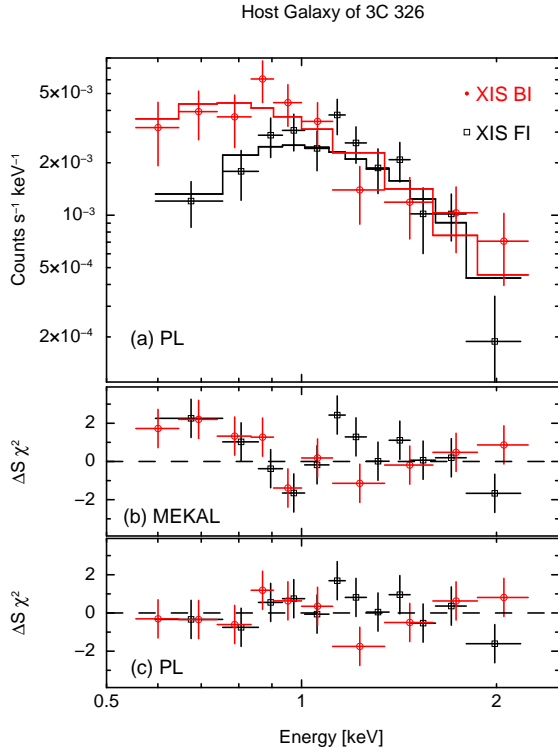


FIG. 4.— *Suzaku* XIS spectrum of the host galaxy of 3C 326. The best-fit PL model is shown in Panel (a), with histograms. The residuals to the MEKAL and PL models are displayed in Panels (b) and (c), respectively.

TABLE 3
SPECTRAL PARAMETERS OF THE HOST GALAXY OF 3C 326

Model	PL	MEKAL
N_{H} (10^{20} cm $^{-2}$)		3.84 ^a
Γ of kT (keV)	$3.38^{+0.35}_{-0.34}$	$1.27^{+0.25}_{-0.19}$
Abundance (solar)	...	0.4
F_{X} (ergs cm $^{-2}$ s $^{-1}$) ^b	6.2×10^{-14}	4.0×10^{-14}
L_{X} (ergs s $^{-1}$) ^c	1.6×10^{42}	8.6×10^{41}
$\chi^2/\text{d.o.f}$	15.8/20	36.1/20

^aFixed at the Galactic value.

^bObserved flux in 0.5 – 2 keV.

^cAbsorption-corrected luminosity in 0.5 – 2 keV at the source rest frame ($z = 0.0895$).

after rejecting that from the region corresponding to the calibration source. X-ray signals were significantly detected in the soft energy band with a 0.5 – 2 keV count rate of $(2.4 \pm 0.2) \times 10^{-3}$ cts s $^{-1}$ and $(3.3 \pm 0.4) \times 10^{-3}$ cts s $^{-1}$ with the XIS FI and BI, respectively. On the other hand, we found that the X-ray signals in the hard energy band were marginal with a count rate of $(7.5 \pm 1.5) \times 10^{-4}$ cts s $^{-1}$ and $(7.8 \pm 2.5) \times 10^{-4}$ in the 3 – 8 keV range. These indicate that the 3C 326 host galaxy exhibits a rather soft X-ray spectrum.

Figure 4 shows the *Suzaku* XIS spectrum of the 3C 326 host galaxy in the 0.5 – 2 keV range. We tried to fit the spectrum with a MEKAL model, modified by the Galactic absorption. The metal abundance was fixed at 0.4 solar, a typical value for nearby elliptical galaxies (Matsushita et al. 2000). The MEKAL model failed to reproduce the observed spectrum ($\chi^2/\text{d.o.f} = 36.1/20$), because of significant residuals below ~ 1 keV (the panel (b) in Figure 4). Although this may suggest an additional low-temperature component, we did not examine a two-temperature MEKAL model, due to insufficient signal statistics. In order to estimate the flux and luminosity, we replaced the MEKAL model with a simple PL model modified by the Galactic absorption. The PL model successfully approximated the data ($\chi^2/\text{d.o.f} = 15.8/20$), with spectral parameters shown in Table 3. The X-ray flux was measured to be 6.2×10^{-14} ergs cm $^{-2}$ s $^{-1}$ in 0.5 – 2 keV, which corresponds to an absorption-corrected luminosity of 1.6×10^{42} ergs s $^{-1}$ at the redshift of 3C 326.

3.5. X-ray spectrum of contaminating sources

As shown in Figure 1, the XIS detected several contaminating X-ray sources. In the following, we briefly analyse their X-ray spectra, although we regard detailed discussion on their nature to be beyond the scope of the present paper.

3.5.1. The unidentified source WARP J1552.4+2007

The X-ray spectrum of an unidentified X-ray source WARP J1552.4+2007 (Perlman et al. 2002), the brightest source in this field, was extracted within the circle of a $2'.5$ arcmin radius, centered on the X-ray peak (the white triangle in Figure 1). The XRB and NXB were subtracted, utilizing the events in the SF region, with the calibration source region removed. Figure 5 shows the background-subtracted XIS spectra of the source, in which the X-ray signals are significantly detected in the 0.3 – 8 keV range.

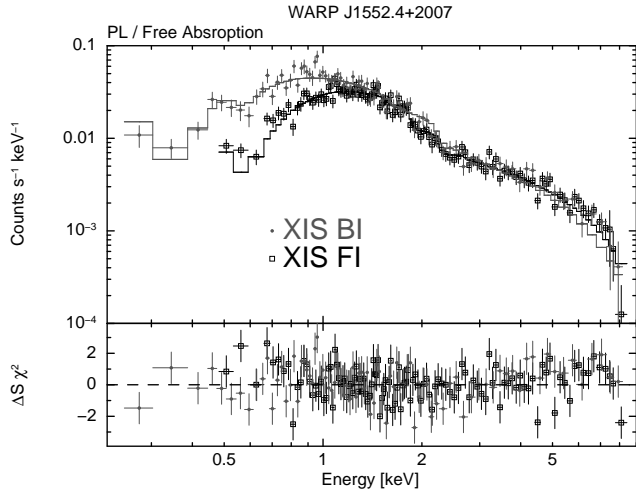


FIG. 5.— *Suzaku* XIS spectrum of an unidentified X-ray source, WARP J1552.4+2007, shown with the best-fit PL model with histograms.

Since no spectral features are seen, we examined a simple PL model modified by free absorption. We obtained a reasonable fit ($\chi^2/\text{d.o.f} = 233.7/197$) with parameters summarized in Table 4. The fit suggests some residuals above $\gtrsim 6$ keV, although we do not investigate this in detail. The absorption column density was consistent with the Galactic value. The X-ray flux of WARP J1552.4+2007 was measured as $F_X = 8.6 \times 10^{-13}$ ergs cm^{-2} s^{-1} in 2 – 10 keV. The X-ray spectrum alone does not yield further insight into the nature of the source.

3.5.2. The quasar [HB89] 1543+203

In order to reduce the contamination from diffuse emission associated with the cluster of galaxies WARP J1552.2+2013, a small circle of a $1'.5$ arcmin radius centered on [HB89] 1543+203 (the white inverted triangle in Figure 1) was adopted. We subtracted the X-ray spectrum from the SF region, in the manner similar to WARP J1552.4+2007. Because the calibration source irradiates the top corner of the XIS BI, we limited the BI data to below 5 keV. As shown in Figure 6, the X-ray signals are significantly detected over 0.4 – 8 keV.

We successfully reproduced the XIS spectrum of the quasar ($\chi^2/\text{d.o.f} = 75.3/83$) by a simple PL model modified with an absorption, whose column density is consistent with the Galactic value. The obtained parameters

TABLE 4
SUMMARY OF THE PL FITTING TO THE *Suzaku* XIS SPECTRA OF WARP J1552.4+2007 AND [HB89] 1543+203.

Source	WARP J1552.4+2007	[HB89] 1543+203
$N_{\text{H}}(10^{20} \text{ cm}^{-2})$	$4.2^{+0.9}_{-0.8}$	$6.3^{+2.7}_{-2.5}$
Γ	$1.97^{+0.05}_{-0.04}$	$2.13^{+0.11}_{-0.10}$
F_X (ergs cm^{-2} s^{-1}) ^a	8.6×10^{-13}	4.4×10^{-13}
L_X (ergs s^{-1}) ^b	...	8.5×10^{43}
$\chi^2/\text{d.o.f}$	233.7/197	75.3/83

^aAbsorption-inclusive 2 – 10 keV flux

^bAbsorption-corrected 2 – 10 keV luminosity, at the source rest frame.

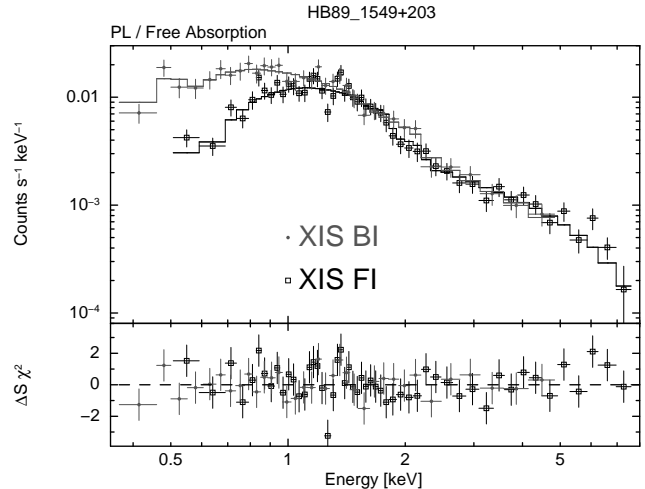


FIG. 6.— *Suzaku* XIS spectrum of the quasar, [HB89] 1543+203, on which the best-fit PL model is overlaid.

are listed in Table 4. The measured 2 – 10 X-ray flux, $F_X = 4.4 \times 10^{-13}$ ergs cm^{-2} s^{-1} , corresponds to an X-ray luminosity of $L_X = 8.5 \times 10^{43}$ ergs s^{-1} , at the redshift of the quasar, $z = 0.25$. Using the *Einstein* observatory in 1981, the X-ray flux of [HB89] 1543+203 was measured as $(1.37 \pm 0.11) \times 10^{-12}$ in the 0.3 – 3.5 keV range, after the Galactic extinction was corrected (Gioia et al. 1990). Because the absorption-corrected *Suzaku* flux in the same energy range was estimated to be 8.2×10^{-13} ergs cm^{-2} s^{-1} , the source X-ray intensity has varied by a factor of 1.7, in 27 years between the *Einstein* and *Suzaku* observations.

3.5.3. The cluster of galaxies WARP J1552.2+2013

As shown in Figure 1, a number of member galaxies (filled circles) of the cluster WARP J1552.2+2013 (Perlmutter et al. 2002) are within the XIS FoV, and associated diffuse emission is clearly seen. The X-ray spectrum of this cluster was taken from the circle denoted as C1 in Figure 1. The circle of a $2'$ radius centered on [HB89] 1543+203, and the region corresponding to the calibration source on the XIS BI were rejected from the C1 circle. The SF region was adopted to subtract the NXB + XRB spectrum, in the same way as for WARP J1552.4+2007 and [HB89] 1543+203. The XIS spectrum of the cluster in the 0.4 – 7 keV range is shown

TABLE 5
SPECTRAL PARAMETERS TO THE *Suzaku* XIS SPECTRA OF THE CLUSTER WARP J1552.2+2013.

Parameter	Value
$N_{\text{H}}(10^{20} \text{ cm}^{-2})$	3.84 ^a
kT (keV)	4.1 ± 0.5
A	$0.58^{+0.35}_{-0.28}$
F_X (ergs cm^{-2} s^{-1}) ^b	6.9×10^{-13}
L_X (ergs s^{-1}) ^c	3.5×10^{43}
$\chi^2/\text{d.o.f}$	77.5/82

^aFixed at the Galactic value.

^bAbsorption-inclusive 0.5 – 10 keV flux.

^cAbsorption-corrected 0.5 – 10 keV luminosity, at the source rest frame ($z = 0.136$).

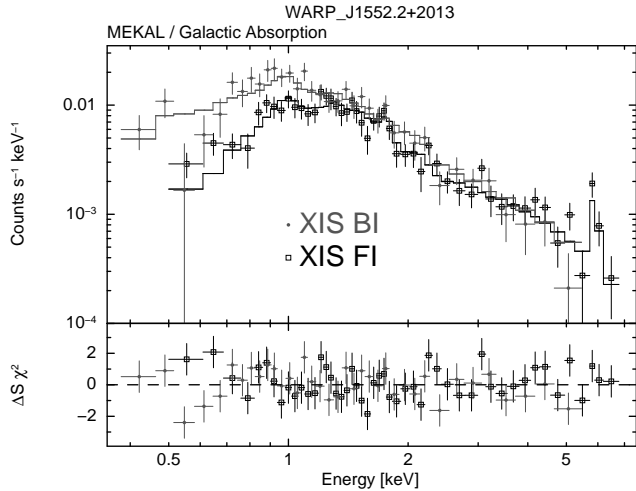


FIG. 7.— *Suzaku* XIS spectrum of the cluster of galaxies, WARP J1552.2+2013. The histograms show the best-fit MEKAL model.

in Figure 7.

We found an emission line feature around ~ 5.8 keV. This energy, corresponding to ~ 6.6 keV at the rest frame of the cluster ($z = 0.136$), is consistent with the energy of the ionized Fe emission lines. We, then, fitted the spectrum with a MEKAL model modified with the Galactic absorption ($\chi^2/\text{d.o.f} = 77.5/82$), and summarise the derived parameters in Table 5. The metal abundance ($A = 0.58^{+0.35}_{-0.28}$) and temperature ($kT = 4.1 \pm 0.5$ keV) are typical for cluster emission (Fukazawa et al. 2004). The X-ray luminosity of the cluster ($L_X = 3.5 \times 10^{43}$ ergs s^{-1} in the 0.5 – 10 keV range) may be slightly lower than that estimated from the luminosity-temperature relation of the typical clusters ($L_X \gtrsim 10^{44}$ ergs s^{-1} ; Fukazawa et al. 2004), although we have to note that the XIS FoV did not cover the whole area of WARP J1552.2+2013.

4. DISCUSSION

4.1. Energetics in the west lobe

We show the spectral energy distribution of 3C 326 in Figure 8 in νF_ν units. The radio spectrum of the west lobe is reported to exhibit a photon index of $\Gamma_R = 1.7 - 1.9$ between 326 MHz and 4.8 GHz (Mack et al. 1997, 1998). The X-ray photon index of the west lobe, which we determined from the *Suzaku* observation, is consistent with this value. This agreement strongly supports that the X-ray emission is produced by the synchrotron-emitting non-thermal electrons in the west lobe, which approximately have a PL-like energy distribution. As is clear from Figure 8, the synchrotron spectrum of the west lobe shows a significant cut-off around 10 GHz, and is expected not to extend to the X-ray frequencies. Therefore, we safely attributed the diffuse X-ray emission from the west lobe to instead be of IC origin. Like in the case of the southern inner lobe of Centaurus A (e.g., Croston et al. 2009), the observed X-ray flux could be contaminated by synchrotron emission from high energy electrons accelerated in the shock region produced by the lobe expansion, and thermal emission from the shocked and/or compressed plasma around the lobe. However, a simple scaling of physical parameters from Centaurus A

TABLE 6
ENERGETICS IN THE WEST LOBE OF 3C 326

Parameters	Value ^a	Systematic errors from		
		S_R	Γ_R	V
u_e (10^{-13} ergs cm^{-3})	$2.3 \pm 0.3 \pm 0.3$	± 0	± 0.3	$+0.6$ -0.4
u_m (10^{-14} ergs cm^{-3})	$1.2^{+0.2}_{-0.1} \pm 0.2$	$+0.2$ -0.1	$+0.5$ -0.4	± 0
B (μG)	$0.55^{+0.04+0.05}_{-0.03-0.04}$	$+0.03$ -0.04	$+0.10$ -0.09	± 0
u_e/u_m	$18.8^{+4.9+5.7}_{-4.3-4.9}$	$+2.6$ -2.1	$+12.2$ -7.0	$+4.7$ -3.5

^aThe first and second errors represent those propagated from the statistical and systematic ones in S_X , respectively.

to 3C 326 by the size assures that the X-ray flux of these components is far from detectable, in this observation.

Among known radio galaxies with lobes detected through the IC X-ray emission, 3C 326 has the largest physical size (~ 2 Mpc). In lobes of radio galaxies on such a large scale ($\gg 100$ kpc) with a low radio surface brightness, the seed photons of the IC process are though to be inevitably dominated by the CMB radiation, rather than other seed photon candidates. These candidates include infra-red (IR) photons from the nucleus (e.g., Brunetti et al. 1997) with an energy density of $\lesssim 10^{-17}$ ergs cm^{-3} , estimated from the upper limit of the nuclear IR luminosity at a wavelength of $15 \mu\text{m}$ of $\sim 1.4 \times 10^{42}$ ergs s^{-1} (Hardcastle et al. 2009), and synchrotron photons themselves with $\sim 10^{-18}$ ergs cm^{-3} from the SR radio flux determined below. Actually, the CMB is evaluated to have a higher energy density of $u_{\text{CMB}} = 5.8 \times 10^{-13}$ ergs cm^{-3} , at the rest frame of 3C 326 ($z = 0.0895$).

We diagnose the energetics in the west lobe of 3C 326, by a comparison between the synchrotron radio and IC X-ray spectra. By examining the linear radio brightness profile from the 1.4 GHz radio map shown in Figure 1, we approximated the shape of the lobe at a sphere with a radius of $140'' \pm 10''$ after deconvolving the beam size ($39'' \times 14''$ in a full width at half maximum). This corresponds to a physical size of 231 ± 23 kpc, which gives a volume of $V = (1.5 \pm 0.3) \times 10^{72}$ cm^3 . We estimated the radio intensity within the X-ray integration region of the west lobe (WL in Figure 1) to be $S_R = 0.85 \pm 0.09$ Jy at 1.4 GHz, from the radio image. This flux is shown with the diamond in Figure 8. Based on the radio data below the GHz range (e.g., Mack et al. 1997, 1998), we adopted the radio photon index of $\Gamma_R = 1.8$ with an error of about ± 0.05 , which corresponds to the slope of the electron number density spectrum to be $p = 2\Gamma_R - 1 = 2.6 \pm 0.1$. In consequence, we re-evaluated the X-ray flux density with the photon index fixed at $\Gamma_R = 1.8$, as $S_X = 19.3 \pm 2.2 \pm 2.6$ nJy at 1 keV (Case 2 in Table 2). We supposed that the magnetic fields are randomly oriented over the lobe. The filling factors of the electrons and magnetic field were assumed to be unity.

We simply referred to Harris & Grindlay (1979), and evaluated the energetics in the west lobe as summarised in Table 6. The energy densities of electrons and magnetic field are calculated as $u_e = (2.3 \pm 0.3 \pm 0.3) \times 10^{-13}$ ergs cm^{-3} and $u_m = (1.2^{+0.2}_{-0.1} \pm 0.2) \times 10^{-14}$ ergs cm^{-3} , respectively. Here, u_e was evaluated for the electrons with a Lorentz factor of $\gamma_e = 10^3 - 10^5$, because they

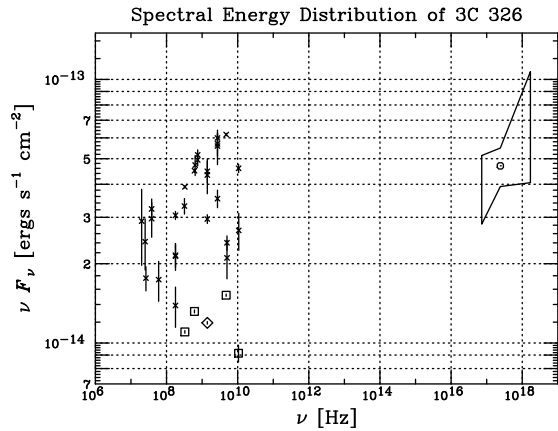


FIG. 8.— Spectral energy distribution of 3C 326. The best-fit PL model to the X-ray spectrum of the west lobe (Case 1) and its 1 keV flux density are plotted by the bow tie and circle, respectively. Only the statistical errors are taken into account for the X-ray spectrum. The crosses indicate the radio spectrum of the whole radio structure between 20 MHz to 10.7 GHz (Aslanian et al. 1968; Braude et al. 1970; Kellermann & Pauliny-Toth 1969, 1973; Kuhr et al. 1979; Mack et al. 1997; Pilkington & Scott 1965; Viner & Erickson 1975; Wright & Otrupcek 1990). The radio spectrum of the west lobe (Mack et al. 1998, the “center” region in their paper) are shown with the boxes. The diamond presents the 1.4 GHz radio flux within the WL region, which was evaluated from the radio image in Figure 1.

are directly visible through the synchrotron radio and/or IC X-ray emission. The first and second errors are due to the statistical and systematic ones of the X-ray flux density, S_X . We found an electron dominance of $u_e/u_m = 18.8^{+4.9+5.7}_{-4.3-4.9}$. As a result, the magnetic field, $B = 0.55^{+0.04+0.05}_{-0.03-0.04} \mu\text{G}$, was slightly weaker than that evaluated under the minimum energy condition (e.g.; Miley 1980) of $B_{\text{me}} \gtrsim 1.1 \mu\text{G}$, neglecting the proton contribution. Even though all the possible systematics, compiled in Table 6, are considered, the electron dominance in the west lobe of 3C 326 is justified.

4.2. Low luminosity nucleus in 3C 326

Recent studies with *Chandra* and *XMM-Newton* (e.g., Evans et al. 2006; Belsole et al. 2006; Hardcastle et al. 2006, 2009) revealed that nuclei of FR II NLRGs exhibit both soft and hard spectral components, the latter of which are heavily absorbed with a column density of $N_{\text{H}} \gtrsim 10^{23} \text{ cm}^{-2}$. Adopting a PL spectrum with a photon index of $\Gamma = 1.7$ subjected to a column density of $N_{\text{H}} = 10^{23} \text{ cm}^{-2}$ (typical values for NLRG nuclei), the marginal signals above 2 keV placed an upper limit on the absorption-corrected 2 – 10 keV X-ray luminosity of the 3C 326 nucleus as $2 \times 10^{42} \text{ ergs s}^{-1}$. Because this upper limit is lower than the typical luminosity of NLRG nuclei by an order of magnitude, ($\gtrsim 10^{43} \text{ ergs s}^{-1}$, Evans et al. 2006; Belsole et al. 2006; Hardcastle et al. 2006), the activity of 3C 326 is suggested to be relatively weak, among NLRGs.

In terms of the de-absorbed X-ray luminosity, the soft X-ray component from NLRG nuclei is found to be dominated by the hard obscured one, typically by an order of magnitude (Evans et al. 2006; Belsole et al. 2006; Hardcastle et al. 2006). In the case of 3C 326, the upper limit on the hard absorbed component luminosity corresponds

to the contribution of the nuclear soft X-ray emission to be less than $\sim 10^{41} \text{ ergs s}^{-1}$. The observed soft X-ray luminosity from the 3C 326 host galaxy, $1.6 \times 10^{42} \text{ ergs s}^{-1}$, highly exceeds this value. In addition, the 0.5 – 2 keV X-ray spectrum of 3C 326 with a photon index of $\Gamma = 3.38^{+0.35}_{-0.34}$ is softer than those of the soft component in NLRG nuclei, $\Gamma \sim 2$ (at most $\Gamma < 3$, Evans et al. 2006; Belsole et al. 2006; Hardcastle et al. 2006). These indicate that a large part of the soft emission observed from the 3C 326 host galaxy is not of nuclear origin. Because the soft component from NLRG nuclei is considered to originate in jets (Hardcastle & Worrall 1999), it is implied that the jet from 3C 326 appears to exhibit only a weak activity, although other origins (e.g., Torresi et al. 2009) for the soft component are not yet ruled out.

The relatively large integration circle with a radius of 149 kpc at the rest frame of 3C 326, due to the *Suzaku* angular resolution, inevitably allows a significant contribution from the thermal emission associated with the host galaxy. Actually, the observed X-ray luminosity, $1.6 \times 10^{42} \text{ ergs s}^{-1}$, is compatible with those of the thermal plasma in nearby elliptical galaxies (Matsushita et al. 2000). Therefore, we attributed the soft X-ray emission from 3C 326 to be dominated by a thermal plasma emission from the host galaxy, although its companion galaxy, which locates $\sim 25''$ north of 3C 326 ($z = 0.0885$; Rawlings et al. 1990), may contribute to some extent.

In order to reinforce the low luminosity nucleus in 3C 326, suggested by the *Suzaku* observation, we show other observational supports in the following. The host galaxy of 3C 326 is reported to exhibit no significant emission line of [OIII] (at a wavelength of $\lambda = 5007 \text{ \AA}$) with an upper limit of $\sim 2 \times 10^{40} \text{ ergs s}^{-1}$ (Saunders et al. 1989). This emission line is regarded as one of the important signatures of activity of galactic nuclei. Using the correlation between the X-ray and [OIII] luminosities for nearby Seyfert galaxies (Panessa et al. 2008), the upper limit on the nuclear X-ray luminosity of 3C 326 is estimated to be $L_X \sim 1 \times 10^{42} \text{ ergs s}^{-1}$ in the 2 – 10 keV range. Recently, Hardcastle et al. (2009) reported another evidence for inactivity of the 3C 326 nucleus from IR observations. They measured an upper limit on its IR luminosity to be $\sim 1.4 \times 10^{42} \text{ ergs s}^{-1}$, at a wavelength of $15 \mu\text{m}$. The correlation between the X-ray and IR luminosities, recently found for local Seyferts (Gandhi et al. 2009), translates this into an upper limit on the 2 – 10 keV X-ray luminosity of $L_X \sim 1 \times 10^{42} \text{ ergs s}^{-1}$. All of these are consistent with our result.

Figure 1 displays a radio source at the center of the 3C 326 host galaxy. However, the radio core of 3C 326 is reported to exhibit a rather low 5 GHz luminosity ($L_{5\text{GHz}} \sim 1 \times 10^{40} \text{ ergs s}^{-1}$) among NLRGs ($L_{5\text{GHz}} = 10^{39} - 10^{42} \text{ ergs s}^{-1}$; Hardcastle & Worrall 1999; Hardcastle et al. 2009). A correlation was reported for NLRGs between the 178 MHz luminosity of the whole radio structure and the X-ray luminosity of the nuclear hard component (Hardcastle et al. 2006, 2009). Adopting this correlation, the 178 MHz luminosity of 3C 326 ($\sim 8 \times 10^{41} \text{ ergs s}^{-1}$, Hardcastle et al. 2009) gives an estimate to the 2 – 10 keV absorption-corrected luminosity as $\sim 10^{43} \text{ ergs s}^{-1}$, which is a factor of 10 larger than the derived upper limit. Thus, the nucleus of 3C 326, including its jets, seems less active for its radio

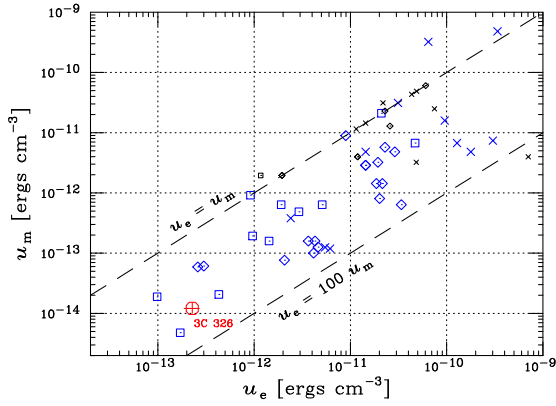


FIG. 9.— The relation between u_e and u_m , determined through the IC technique (Croston et al. 2005; Isobe 2002; Isobe et al. 2002, 2005, 2006; Tashiro et al. 1998, 2009). For the result on the west lobe of 3C 326 shown with the red circle, the propagation from the statistical and systematic errors in S_X are considered. Crosses, diamonds, and squares corresponds to lobes of radio galaxies, with $D < 200$ kpc, $D = 200 - 400$ kpc, and $D > 400$ kpc, respectively. Lobes, from which only the upper limit of IC X-ray flux was obtained, are indicated by the small black points, while the others are shown as the large blue ones. The two dashed lines represents $u_e/u_m = 1$ and 100.

lobe luminosity. Because the extended lobes trace the past activity of the jet emanating from the nucleus, the 3C 326 nucleus is considered to have been more active in the past, and to become relatively weak, recently. A similar decline in the nuclear activity was reported from the radio galaxy Fornax A (Iyamoto et al. 1998), with a current 0.3 – 8 keV luminosity of $L_X = 5 \times 10^{39}$ ergs s^{-1} (Kim & Fabbiano 2003).

4.3. Evolution of lobe energetics

In order to investigate evolution of the lobe energetics, we compared 3C 326 with other radio galaxies accompanied by smaller lobes. Figure 9 summarizes u_e and u_m in lobes of radio galaxies, determined through IC X-ray technique (Croston et al. 2005; Isobe 2002; Isobe et al. 2002, 2005, 2006; Tashiro et al. 1998, 2009). We confirmed that almost all the radio lobe are distributed between the lines of $u_e/u_m = 1$ and 100 (e.g., Isobe et al. 2005; Croston et al. 2005), over a wide range of u_e and u_m . The west lobe of 3C 326 fully follows this trend. Moreover, Figure 9 indicates that radio galaxies on a larger scale tend to exhibit a smaller value of u_e and u_m in their lobes, while the degree of electron dominance u_e/u_m seems to be independent of the size.

The dependence of u_e and u_m on the total dimension D of the radio galaxies is more clearly visualised in Figure 10. Recently, Nagai (2008) reported a trend that the total size of radio sources is almost proportional to the source age ($\tau = 100$ yr – 10 Myr), estimated by the synchrotron aging technique, over a wide range of $D = 10$ pc – 1 Mpc. This proportionality is thought to be justified by the fact that the observed expansion speed of lobes are distributed in a relatively narrow range of $0.01c - 0.1c$ (e.g., Alexander & Leahy 1987; Nagai et al. 2006). Thus, the figure can be regarded as a plot between u_e , u_m and τ . For lobes with $D < 1$ Mpc, we found relations of $u_e \propto D^{-2.2 \pm 0.4}$ and $u_m \propto D^{-2.4 \pm 0.4}$ (the dashed lines in Figure 10), although the data points have a slightly

large scatter (about less than an order of magnitude) around the correlation line. In order to derive the relation, we ignored the lobes in which only the upper limit of u_e (and hence the lower limit of u_m) was derived. The data point of the giant radio galaxy 3C 326 ($D = 1.99$ Mpc) seems to agree with this tendency for the smaller source with $D < 1$ Mpc, within a factor of 2.

The observed correlation could be an artifact, due to the inclination angle, θ , of the radio source axis to the sky plane. As θ increase, the apparent dimension and depth of non-spherical sources becomes shorter and longer, respectively. In addition, the longer depth of the emitting region can enhance the X-ray and radio surface brightness. However, we think that these effects have no impact on the spatially averaged magnetic field strength B and its energy density u_m , because they are determined from the radio and X-ray fluxes spatially integrated over the region of interest, S_R and S_X respectively, where the θ dependence is canceled out. The spatially averaged electron energy density u_e is proportional to the observed value of $S_X V^{-1}$. Because the apparent volume of the source linearly depends on its apparent dimension, we expect that θ is possible to cause a fake dependence of $u_e \propto D^{-1}$. However, this imitation can not explain the observed relation. Therefore, we regard the observed correlation between u_e , u_m and D to be real.

What does the relation tell us? For simplicity, we assume that the energy input rate by jets to lobes is common among radio galaxies, and constant in time. While the jet is active, we anticipate that the sum of the energy densities, $u_e + u_m$, scales as τD^{-3} , since the total energy with which the jets supplied and the volume of the lobes are thought to be proportional to τ and D^3 , respectively. The proportionality between τ and D (Nagai 2008) translate the relation into $u_e + u_m \propto D^{-2}$. The dispersion of jet power of FR II radio galaxies (nearly an order of magnitude; Rawlings & Saunders 1991) may blur the relation. After the jets cease transporting sufficient energy to the lobes, a relation of $u_e + u_m \propto D^{-3} \exp(-t/T)$ is expected. Here, t is a time after the end of the jet activity, and $T \sim 0.2$ Gyr $(1+z)^{-4} (1+f)^{-1} (\gamma_e/10^4)^{-1}$ is a cooling time scale of electrons due to synchrotron and IC radiation, with f being a ratio of u_m to the CMB energy density at the source rest frame, $u_{\text{CMB}}(z) = 4.1 \times 10^{-13} (1+z)^4$ ergs cm^{-3} . For $t \ll T$, the radiation energy loss is neglected, and then, the lobe is thought to expand almost adiabatically to establish the pressure balance with its environment. In this second stage, the lobe is expected to follow a condition of $u_e + u_m \propto D^{-3}$. On the other hand, in the final stage when the time-integrated energy loss become significant ($t \gg T$), we presume that u_e and u_m decrease rapidly. As a result, the lobe moves downward in the $D-u_e$ and $D-u_m$ plots.

The observed relations of $u_e \propto D^{-2.2 \pm 0.4}$ and $u_m \propto D^{-2.4 \pm 0.4}$ for the radio galaxies with $D < 1$ Mpc is close to that expected in the active phase of the jets on the above argument. The fact that 3C 326 agrees with these correlations within a factor of ~ 2 , clearly shown in Figure 10, suggests that even the lobes of giant radio galaxies with a size of $D > 1$ Mpc are supplied with a sufficient energy comparable to those into lobes with a moderate size ($D \sim 100$ kpc), at least for the case of 3C 326. However, this argument apparently conflicts with only a weak

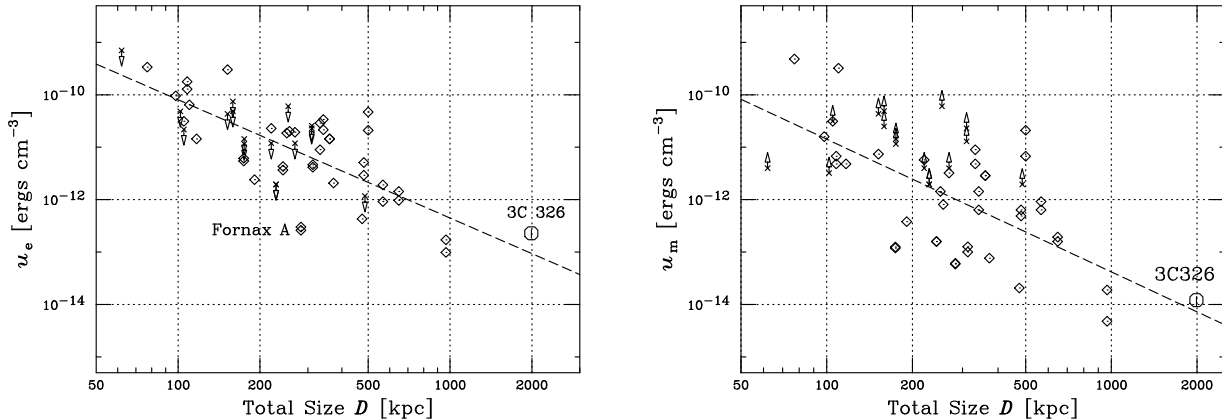


FIG. 10.— The energy densities of electrons (left) and magnetic fields (right), u_e and u_m respectively, in lobes (Croston et al. 2005; Isobe 2002; Isobe et al. 2002, 2005, 2006; Tashiro et al. 1998, 2009), plotted against the total size, D , of radio galaxies. The circle corresponds to the west lobe of 3C 326, for which the statistical and systematic errors in S_X are taken into account. Diamonds shows lobes from which the IC X-rays were securely detected, while crosses indicate those with only the upper limit on the IC flux. The dashed lines represent the best-fit relations of $u_e \propto D^{-2.2}$ and $u_m \propto D^{-2.4}$, for lobes displayed with diamonds.

activity of the 3C 326 nucleus, which we suggested in this *Suzaku* observation. In order to reconcile this inconsistency, it is suggested that the 3C 326 nucleus had been more active, and dimmed very recently. As a result, it is implied that the rear end of the jet may have not yet arrived at the hot spot, where the bulk jet energy is randomized and injected into the lobe. Adopting the typical speed of kpc-scale jets in FR II radio galaxies, $0.5c - 0.7c$ (Hardcastle et al. 1999), it takes ~ 5 Myr for the jets to travel a distance of ~ 1 Mpc from its nucleus. Therefore, we regard that it has been at most 5 Myr (neglecting the light travel time from the source to the Earth), since the nucleus of 3C 326 declined its activity. This means that the west lobe of 3C 326 is about to make a transition into the second stage.

In Figure 10, we notice that one radio galaxy, Fornax A, deviates significantly below the trend of other radio galaxies by more than an order of magnitude, especially in the u_e - D plot. As mentioned in §4.2, Iyomoto et al. (1998) reported the dormancy of its nucleus, based the *ASCA* observation. They estimated that it has been ~ 0.1 Gyr, since the end of its nuclear activity. This is comparable to (or a few times) the electron life time in the lobes. All of these indicate that Fornax A has already entered the final stage.

We have just started to reveal the evolution of the

energetics in lobes of radio galaxies, through IC X-ray observations on a large physical extent ($D > 1$ Mpc). However, our current knowledge is far from conclusive. We regard it important to enlarge the X-ray sample of giant radio galaxies, and to fill the gap in the region of $D = 0.5 - 2$ Mpc in Figure 10.

We are grateful to all the members of the *Suzaku* team, for the successful operation and calibration. We thank the anonymous referee for her/his great interest to the results and valuable comments to finalize the present paper. Theoretical discussions with Dr. Kino improved the draft. N. I. is supported by the Grant-in-Aid for the Global COE Program, "The Next Generation of Physics, Spun from Universality and Emergence" from the Ministry of Education, Culture, Sports, Science and Technology (MEXT) of Japan. P. G. acknowledges the RIKEN Foreign Postdoctoral Researcher Fellowship. We have made extensive use of the NASA/IPAC Extra galactic Database (NED; the Jet Propulsion Laboratory, California Institute of Technology, the National Aeronautics and Space Administration). The unpublished 1.4 GHz radio image of 3C 326 was downloaded from "An Atlas of DRAGNs" ⁷, edited by Leahy, Bridle, & Strom.

⁷ <http://www.jb.man.ac.uk/atlas/>

REFERENCES

- Alexander, P., & Leahy, J. P., 1987, *MNRAS*, 225, 1
 Aslanian, A. M., Dagkesamanskii, R. D., Kozhukhov, V. N., Malumian, V. G., & Sanamian, V. A., 1968, *Astrofizica*, 4, 129
 Belsole, E., Worrall, D. M., & Hardcastle, M. J., 2006, *MNRAS*, 366, 339
 Braude, S. Y., Lebedeva, O. M., Megn, A. V., Ryabov, B. P., & Zhouck, I. N., 1970, *Astrophys. Lett.*, 5, 129
 Brunetti, G., Setti, G., & Comastri, A., 1997, *A&A*, 325, 898
 Croston, J. H., Hardcastle, M. J., Harris, D. E., Belsole, E., Birkinshaw, M., Worrall, D. M., 2005, *ApJ*, 626, 733
 Croston, J. H., et al. 2009, *MNRAS*, 395, 1999
 Dickey, J. M., & Lockman, F. J. 1990, *ARA&A*, 28, 215
 Evans, D. E., Worrall, D. M., Hardcastle, M. J., Kraft R. P., & Birkinshaw M., 2006, *ApJ*, 642, 96
 Fanaroff, B. L., & Riley, J. M., 1974. *MNRAS*, 167, 31
 Feigelson, E. D., Laurent-Muehleisen, S. A., Kollgaard, R. I., & Fomalont, E. B., 1995, *ApJ*, 449, L149
 Fukazawa et al., 2004, *PASJ*, 56, 965
 Fukazawa, F., et al., 2009, *PASJ*, 61, 17
 Gandhi et al. 2009, *A&A*, in press (arXiv:0902.2777)
 Gioia, I. M., Maccacaro, T., Schild, R. E., Wolter, A., Stocke, J. T., Morris, S. L., & Henry, J. P., 1990, *ApJS*, 72, 567,
 Harris, D. E., & Grindlay, J. E., 1979, *MNRAS*, 188, 25
 Hardcastle, M. J., Alexander P., Pooley, G. G., & Riley, J. M., 1999, *MNRAS*, 204, 135
 Hardcastle, M. J., Evans, D. A., & Croston, J. H., 2006, *MNRAS*, 370, 1893
 Hardcastle, M. J., Evans, D. A. & Croston, J. H. 2009, *MNRAS*, 396, 1929
 Hardcastle, M. J., & Worrall, D. E., 1999, *MNRAS*, 309, 969

- Isobe, N., 2002, PhD thesis, University of Tokyo
- Isobe, N., et al., 2002, *ApJ*, 580, L111
- Isobe, N., Makishima, K., Tashiro, M., & Hong, S., 2005, *ApJ*, 632, 781
- Isobe, N., Makishima, K., Tashiro, M., Itoh, K., Iyomoto, N., Takahashi, I., & Kaneda, H., 2006, *ApJ*, 645, 256
- Iyomoto, N., Makishima, K., Tashiro, M., Inoue, S., Kaneda, H., Matsumoto, Y., & Mizuno, T. 1998, *ApJ*, 503, L31
- Ishisaki, Y., et al. 2007, *PASJ*, 59, 113
- Kaneda, H., et al., 1995, *ApJ*, 453, L13
- Kataoka, J., Stawarz, L., 2005, *ApJ*, 622, 797
- Kellermann, K. I., & Pauliny-Toth, I. I. K., 1969, *ApJ*, 157, 1
- Kellermann, K. I., & Pauliny-Toth, I. I. K., 1973, *AJ*, 78, 828
- Kim, Dong-Woo, & Fabbiano, G., 2003, *ApJ*, 586, 826
- Klein, U., Mack, K.-H., Strom, R., Wielebinski, R., & Achatz, U., 1994, *A&A*, 283, 729
- Kokubun, M., et al., 2007, *PASJ*, 59, S53
- Konar, C., Hardcastle, M. J., Croston, J. H., Saikia, D. J., 2009, *MNRAS*, in press, (arXiv:0908.0426)
- Koyama K., et al., 2007, *PASJ*, 59, S23
- Kuhr, H., Nauber, U., Pauliny-Toth, I. I. K., & Witzel, A. 1979, *A Catalogue of Radio Sources (Bonn: Max-Planck Institut fur Radio Astronomie)*
- Kushino, A., Ishisaki, Y., Morita, U., Yamasaki, N. Y., Ishida, M., Ohashi, T., & Ueda, Y., 2002, *PASJ*, 54, 327
- Lumb, D. H., Warwick, R. S., Page, M., & De Luca, A., 2002, *A&A*, 389, 93
- Mack, K.-H., Klein, U., O'Dea, C. P., & Willis A. G., 1997, *A&AS*, 123, 423
- Mack, K.-H., Klein, U., O'Dea, C. P., Willis, A. G., & Saripalli, L., 1998, *A&A*, 329, 431
- Matsushita, K., Ohashi, T., & Makishima, K., 2000, *PASJ*, 52, 685
- Mewe, R., Gronenschild, E. H. B. M., & van den Oord, G. H. J. 1985, *A&AS*, 62, 197
- Migliori, G., Grandi, P., Palumbo, G. G. C., Brunetti, G. & Stanghellini, C. 2007, *ApJ*, 668, 203
- Miley, G., 1980, *ARA&A*, 18, 165
- Mitsuda, K., et al., 2007, *PASJ*, 59, S1
- Nagai, H., 2008, *The Astronomical Herald (ISSN 0374-2466)*, 101, 264
- Nagai, H., Inoue, M., Asada, K., Kameno, S., & Doi, A., 2006, *ApJ*, 648, 148
- Panessa, F., et al., 2006, *A&A*, 455, 173
- Perlman, E. S., Horner, D. J., Jones, L. R.; Scharf, C. A., Ebeling, H., Wegner, G. & Malkan, M., 2002, *ApJS*, 140, 265
- Pilkington, J. D. H., & Scott, P. F., 1965, *MmRAS*, 69, 183
- Rawlings, S., Saunders, R., Miller, P., Jones, M. E., & Eales, S. A., 1990, *MNRAS*, 246, 21
- Rawlings, S., & Saunders, R., 1991, *Nature*, 349, 138
- Saunders, R., Baldwin, J.E., Rawlings, S., Warner, P.J., & Miller, L., 1989, *MNRAS*, 238, 777
- Serlemitsos, P.J, et al., 2007, *PASJ*, 59, S9
- Spinrad, H., Marr, J., Aguilar, L., & Djorgovski, S. 1985, *PASP*, 97, 93
- Takahashi, T., et al., 2007, *PASJ*, 59, S35
- Tashiro, M., et al., 1998, *ApJ*, 499, 713
- Tashiro, M., Makishima, K., Iyomoto, N., Isobe, N., & Kaneda, H., 2001, *ApJ*, 546, L19
- Tashiro M., Isobe, N., Seta H., Yaji, Y., & Matsuta K., 2009, *PASJ*, 61, S327
- Tawa, N., et al., 2008, *PASJ*, 60, S11
- Torresi E., Grandi, P., Guainazzi, M., Palumbo, G. G. C., Ponti, G., & Bianchi, S., 2009, *A&A*, 498, 61
- Tremblay, G. R., Chiaberge, M., Donzelli, C. J., Quillen, A. C., Capetti, A., Sparks, W. B., & Macchetto, F. D., 2007, *ApJ*, 666, 109
- Vikhlinin, A., McNamara, B. R., Forman, W., Jones, C., Quintana, H., Hornstrup, A., 1998, 502, 558
- Viner, M. R., & Erickson, W. C., 1975, *AJ*, 80, 931
- Wegner, G., & Swanson, S. R., 1990, *AJ*, 100, 1274
- Wright, A., & Otrupcek, R. 1990, *Parkes Catalogue*, Australia Telescope National Facility